Contributions of Valine-292 in the Nicotinamide Binding Site of Liver Alcohol Dehydrogenase and Dynamics to Catalysis[†,‡]

Jon K. Rubach, S. Ramaswamy, and Bryce V. Plapp*

Department of Biochemistry, The University of Iowa, Iowa City, Iowa 52242

Received July 23, 2001; Revised Manuscript Received August 27, 2001

ABSTRACT: The participation of Val-292 in catalysis by alcohol dehydrogenase and the involvement of dynamics were investigated. Val-292 interacts with the nicotinamide ring of the bound coenzyme and may facilitate hydride transfer. The substitution of Val-292 with Ser (V292S) increases the dissociation constants for the coenzymes (NAD^+ by 50-fold, NADH by 75-fold) and the turnover numbers by 3−7-fold. The V292S enzyme crystallized in the presence of NAD^+ and 2,3,4,5,6-pentafluorobenzyl alcohol has an open conformation similar to the structure of the wild-type apo-enzyme, rather than the closed conformation observed for ternary complexes with wild-type enzyme. The V292S substitution perturbs the conformational equilibrium of the enzyme and decreases the kinetic complexity, which permits study of the hydride transfer step with steady-state kinetics. Eyring plots show that the $\Delta H^{\ddagger}$ for the oxidation (V_1) of the protio and deuterio benzyl alcohols is 13 kcal/mol and that the kinetic isotope effect of 4.1 is essentially temperature-independent. Eyring plots for the catalytic efficiency for reduction of benzaldehyde (V_2/K_p) with NADH or NADD are distinctly convex, being temperature-dependent from 5 to 25 °C and temperature-independent from 25 to 50 °C; the kinetic isotope effect of 3.2 for V_2/K_p is essentially independent of the temperature. The temperature dependencies and isotope effects for V_1 and V_2/K_p are not adequately explained by semiclassical transition state theory and are better explained by hydride transfer occurring through vibrationally assisted tunneling.

Valine-292 is located in the nicotinamide binding pocket of the coenzyme binding domain of liver alcohol dehydrogenase (ADH).[1] In ternary complexes of the enzyme with NAD^+ and an alcohol or with NADH and a formamide, the side chain of Val-292 is about 4 Å from the nicotinamide ring, on the face opposite to the one involved in hydride transfer (*1*, *2*). If Val-292 is involved in facilitating hydride transfer, changing this residue should affect catalysis. The Val292Ser substitution (V292S) was found to alter the mechanism and to unmask hydride transfer steps, which permitted study of the contribution of dynamics to catalysis.

Evidence that hydrogen transfer can proceed with quantum mechanical tunneling in various enzymatic reactions has led to a growing awareness that protein dynamics are involved in enzymatic catalysis (*3*, *4*). Theoretical models suggest that hydrogen tunneling can be facilitated by protein or substrate fluctuations, e.g., vibrationally assisted tunneling (*5*−*9*), or without these dynamics, e.g., corner-cutting (*10*). Hydrogen tunneling has been shown to occur in the oxidation of benzyl alcohol catalyzed by yeast alcohol dehydrogenase (*11*), by ADH from *Bacillus stearothermophilus* (*12*), and by horse liver ADH with various amino acids substituted (*13*, *14*). The involvement of tunneling in the reduction of aldehydes and the contribution of the dynamics of horse liver ADH to catalysis need to be determined. Kinetic complexity usually hinders the ability to observe the isotopically sensitive steps of the reaction catalyzed by wild-type ADH, but substitutions of certain amino acids in the enzyme can affect substrate binding and unmask the hydrogen transfer steps (*13*). Temperature dependencies and kinetic isotope effects provide diagnostic information on the mechanism of hydrogen transfer (*3*−*10*, *12*).

EXPERIMENTAL PROCEDURES

Materials. $LiNAD^+$ and Na_2NADH were purchased from Roche Molecular Biochemicals. Benzyl alcohol-α,α-d_2 (98.6% D) was from MSD Isotopes. (4*R*)-[4-^{2}H]NADD was prepared from NAD^+ and ethanol-d_6 (Aldrich, 99+% D) with yeast alcohol dehydrogenase (*15*) and purified on a DEAE-Sepharose column developed with a linear gradient of 10−250 mM sodium phosphate buffer, pH 8. Benzyl alcohol and benzaldehyde were redistilled before use.

Preparation of the Enzyme. The plasmid pBPP/*Eq*ADH (*16*) was used for expression of wild-type *Eq*ADH, and the plasmid pBPP/V292S *Eq*ADH was created for expression of V292S ADH in *Escherichia coli* strain XL1-Blue from Stratagene. Partially random mutagenesis used the Stratagene Quick Change method, with degenerate oligodeoxyribonucleotide mutamers. The mutamers with the following sequences were synthesized by Life Technologies, Inc.: GCA TAT GGT GTG AGC GTA ATT (G/A)(T/C/G)C GGA GTA CCT CCT GAT TCC and CGT ATA CCA CAC TCG CAT TAA (C/T)(A/G/C)G CCT CAT GGA GGA CTA AGG, where the underlines mark the sites of mutation. After

[†] This work was supported by NIH Grants T32 GMO8365 and AA00279 and by NSF Grant MCB 95-06831.

[‡] The X-ray coordinates and structure factors have been deposited in the RCSB Protein Data Bank with the entry name 1JU9.

* Corresponding author. E-mail: bv-plapp@uiowa.edu.

[1] Abbreviations: ADH, alcohol dehydrogenase; *Eq*, *Equus caballus*, horse; V292S, substitution of Val-292 with Ser; KIE, kinetic isotope effect.

10.1021/bi011540r CCC: $20.00 © 2001 American Chemical Society
Published on Web 09/29/2001

transformation in XL1-Blue cells and selection for ampicillin- and tetracycline-resistant colonies, plasmids were isolated, and mutations were identified by the loss of an *Hga*I restriction site (CGCAG). The V292S mutation was confirmed by complete sequencing of the V292S ADH cDNA. The enzyme was purified (*16*) and judged to be more than 95% pure upon electrophoresis of denatured protein in a polyacrylamide gel in the presence of sodium dodecyl sulfate and of native protein in an agarose gel.

Steady-State Kinetics. The concentration of enzyme active sites was determined by titration with NAD^+ in the presence of pyrazole (*17*). The extinction coefficient (at 294 nm) of the complex of NAD^+ and pyrazole with V292S ADH is 6.8 mM^{-1} cm^{-1}. The specific activity of V292S ADH is 49 units/mg, with a turnover number of 34 s^{-1} in the standard assay (*18*). Coenzyme concentrations were determined by absorbance at 260 or 340 nm. Most studies used 33 mM sodium phosphate and 0.25 mM EDTA buffer, pH 8, at 25 °C. Enzyme activities were determined on a Cary 118C spectrophotometer or on an SLM 4800C fluorometer (λ_{ex} = 340 nm, λ_{em} = 460), with computer-fitting of the progress curves to obtain the initial velocities. The isotope effects on steady-state kinetic parameters were obtained by comparing deuterated and nondeuterated substrates, varying both the substrate and coenzyme concentrations, and the data were fitted to the equation for a sequential bi reaction. The steady-state kinetic data were fitted using Clelands' programs (*19*).

Transient Kinetics. A BioLogic SFM3 stopped-flow instrument (dead time of 2.4 ms) was used to study the transient kinetics. Binding of NAD^+ was monitored by the increase in absorbance at 294 nm due to the formation of the enzyme−NAD^+−pyrazole complex, and the binding of NADH was studied by the quenching of protein fluorescence (λ_{ex} = 294 nm, λ_{em} = 310−384 nm) in the presence of *N*-cyclohexylformamide. The rates of coenzyme binding were measured for varied concentrations of NAD^+ and pyrazole or NADH and *N*-cyclohexylformamide. The progress curves were analyzed by the BioKine software and were found to fit a first-order process.

The transient reaction of benzyl alcohol oxidation was studied at a fixed concentration of 5 mM NAD^+, varying the concentration (0.16−5 mM) of benzyl alcohol or benzyl alcohol-α,α-d_2, and by measuring the absorption at 332 nm, near the isosbestic point for free and enzyme-bound NADH (ϵ = 5500 M^{-1} cm^{-1}).

pH Dependency Studies. The pH dependencies of benzyl alcohol oxidation and benzaldehyde reduction at 25 °C, in the range of 5.5−9.5, were studied using 10 mM $Na_4P_2O_7$ and 0.25 mM EDTA buffer adjusted to the desired pH and a final ionic strength of 0.1 with H_3PO_4, NaH_2PO_4, and Na_2HPO_4. Buffers at or above pH 9.5 contained 10 mM $Na_4P_2O_7$, 0.25 mM EDTA, and 5 mM sodium carbonate. The buffers were made at double-strength and diluted 2-fold for the final reaction mixture, using enzyme in weakly buffered solutions. At each pH, V_1 (k_{cat}) and catalytic efficiency, V_1/K_b (k_{cat}/K_m), for benzyl alcohol oxidation were determined by varying the concentration of benzyl alcohol at a fixed concentration of NAD^+ (4 mM) and fitting the data to the Michaelis−Menten equation. The kinetic constants for the reduction of benzaldehyde were determined by varying the concentrations of both benzaldehyde and NADH and fitting the data to the equation for a sequential bi reaction. The pH dependency data were fitted to the appropriate equations using NONLIN (*20*).

Temperature Dependency Studies. Initial velocities were measured over a temperature range of 5−55 °C. The studies were done in 10 mM $Na_4P_2O_7$, 0.25 mM EDTA, at pH values close to the pH-independent regions, pH 9.2 for V_1 and pH 7 for V_2/K_p, to minimize the effects of rate changes due to temperature-dependent shifts in pH. The pH of the buffer was measured at each temperature. Due to the temperature dependence of the pK_a for V_1, to be discussed later, the pH-independent rate for V_1 was used for the fitting of the temperature dependence. The data for the temperature dependencies of V_1 and V_2/K_p were fitted to the logarithmic forms of the Arrhenius and Eyring equations using NONLIN. The logarithm of the data values correctly weights the error, which was proportional to the magnitude of the value. The effect of temperature on V_1 was determined by varying the concentrations of NAD^+ and benzyl alcohol or benzyl alcohol-α,α-d_2 in a constant ratio. The data were fitted using the program NONLIN to eq 1, which is the equation for a sequential bi reaction where *B* is the concentration of alcohol and the ratio of *A*/*B* ([NAD^+]/[benzyl alcohol]) is fixed.

$$v = \frac{VB^2}{a + bB + B^2};\ a = \frac{K_{ia}K_b}{ratio};\ b = \frac{K_a}{ratio} + K_b \qquad (1)$$

The temperature dependence for V_2/K_p was determined by measuring the initial velocities at a concentration of benzaldehyde that was less than 0.05 of the K_p at each temperature, with varied concentrations of NADH or NADD. The data were fitted to the Michaelis−Menten equation (*19*). The same concentration of benzaldehyde was used for both NADH and NADD assays.

X-ray Crystallography. Crystals of the V292S enzyme were produced in hanging drops using 10 mg/mL enzyme in 50 mM ammonium *N*-[tris(hydroxymethyl)methyl]-2-aminoethanesulfonate buffer, pH 7.0, at 5 °C, with 9% 2-methyl-2,4-pentanediol, 10.6 mM NAD^+, and 20 mM 2,3,4,5,6-pentafluorobenzyl alcohol. The well reservoir contained 18% 2-methyl-2,4-pentanediol. The crystallization conditions are the same as used for producing wild-type crystals of the ternary complex with 2,3,4,5,6-pentafluorobenzyl alcohol, except the concentrations of the coenzyme and inhibitor are 10-fold higher. Crystals were flash-cooled, and the data were collected at 100 K with an R-Axis IV++ mounted on a rotating-anode generator. The data sets were processed using MOSFLM (*21*) and scaled using SCALA (*22*). The structure of the V292S enzyme was solved by molecular replacement using AMORE (*23*) and coordinates for the refined wild-type ADH−NAD^+−2,3,4,5,6-pentafluorobenzyl alcohol ternary complex (*1*) as a model. The catalytic domain (residues 1−178, 319−374) and coenzyme binding domain (residues 179−318) were treated independently of each other. A composite-omit map for the dimer was produced with the program CNS (*24*), and the program O (*25*) was used for model building. The structure was refined by cycles of model building and least-squares refinement with REFMAC (*22*). Model bias was avoided during the initial refinement by making residue 292 an Ala, and by not adding NAD^+ or 2,3,4,5,6-pentafluorobenzyl alcohol to the model. The structure was checked using WHATIF (*26*) and Procheck (*27*).

Table 1: Steady-State Kinetic Constants for Recombinant Wild-Type and V292S Enzymes[a]

kinetic constant	rADH	V292S ADH
K_a (μM)	3.7	140
K_b (μM)	23	220
K_p (μM)	30	440
K_q (μM)	1.7	80
K_{ia} (μM)	31	1640
K_{iq} (μM)	0.4	30
V_1 (s^{-1})	2.2	6.3
V_2 (s^{-1})	22	160
V_1/K_b ($mM^{-1}\,s^{-1}$)	96	28
V_2/K_p ($mM^{-1}\,s^{-1}$)	700	360
K_{eq} (pM)[b]	44	32
turnover number (s^{-1})[c]	1.1	34

[a] Kinetic constants were determined at 25 °C in 33 mM sodium phosphate and 0.25 mM EDTA buffer, pH 8.0. K_a, K_b, K_p, and K_q are the Michaelis constants for NAD^+, benzyl alcohol, benzaldehyde, and NADH, respectively. K_{ia} and K_{iq} are the dissociation constants for NAD^+ and NADH, respectively. V_1 is the turnover number for benzyl alcohol oxidation, and V_2 is the turnover number for benzaldehyde reduction. The standard errors of fits were <25%. [b] K_{eq} is the Haldane relationship calculated from $V_1K_pK_{iq}[H^+]/V_2K_bK_{ia}$. Values for the equilibrium constant have been estimated to be 35−70 pM (*28*−*30*). [c] Turnover number determined in a standard enzyme assay at 25 °C (*18*), based on titration of active sites.

RESULTS

Kinetic Mechanism. Initial velocity data for the forward and reverse reactions with systematically varied concentrations of coenzyme and substrate were collected for the recombinant wild-type and V292S enzymes and fitted to the equation for a sequential bi reaction. The V292S substitution increases by 3-fold the turnover number for the oxidation of benzyl alcohol and by 7.3-fold the turnover number for the reduction of benzaldehyde (Table 1). The affinity for coenzymes, as measured by inhibition constants, decreases substantially (K_{ia}, NAD^+, by 50-fold; K_{iq}, NADH, by 70-fold). V_1/K_b and V_2/K_p decrease somewhat from the values of the wild-type enzyme, by 3.4-fold and 2-fold, respectively. The results indicate that the V292S substitution significantly affects the kinetics of the enzyme, especially coenzyme binding.

Results of product and dead-end inhibition studies are consistent with an ordered bi-bi mechanism (Table 2). The dissociation constants for the dead-end inhibitors binding to the V292S and wild-type enzymes are very similar. The K_i for *N*-cyclohexylformamide, an aldehyde analogue, with the V292S enzyme is 12 μM, whereas the K_i with the wild-type enzyme is 9 μM (*2*). The dissociation constants for 2,3,4,5,6-pentafluorobenzyl alcohol are 2 μM for V292S ADH and 3 μM for wild-type (*31*). Adenosine monophosphate binds with very similar affinity to both enzymes; for wild-type, the K_i is 44 μM (*32*), and for V292S enzyme, the K_i is 86 μM. This suggests that the decrease in coenzyme binding affinity is not due to effects on the binding of the AMP moiety of the coenzyme. Once the coenzyme is bound, inhibitors bind equally well to the V292S and wild-type enzymes.

The transient kinetics and isotope effects were studied to determine the rate of hydride transfer from benzyl alcohol and the kinetic basis for the large changes in coenzyme affinity. Stopped-flow experiments show that the bimolecular rate constants for binding of NAD^+ and NADH to the V292S enzyme decrease 10-fold and 1.5-fold, respectively, as compared to the wild-type enzyme (Table 3). The rate constants calculated for dissociation of the complexes of enzyme with NAD^+ or NADH are 180 and 220 s^{-1}, respectively (Table 3). The k_{off} for NADH is 40-fold larger and the k_{off} for NAD^+ is 3-fold larger than the respective rate constants for dissociation of coenzyme from the wild-type enzyme. Release of coenzyme is rate-limiting for catalysis by wild-type enzyme (*35*), but the increased dissociation rate constants for the V292S enzyme suggest that the faster turnover numbers are due to faster release of coenzyme and that hydrogen transfer may have become more rate-limiting.

The transient oxidation of benzyl alcohol by the V292S enzyme has no observable burst phase and gives a rate constant at saturating concentrations of substrates (k_{max}) of 6.3 s^{-1} (Table 3), which is the same as the steady-state turnover number. The k_{max} for V292S is 4-fold smaller than that of the wild-type enzyme. The isotope effect on k_{max} is larger than the KIE on k_{max} for wild-type ADH and has the same value as the KIE on V_1 (Table 3). The substrate isotope effects for V_1 and V_1/K_b are 3-fold larger for the V292S enzyme as compared to the wild-type enzyme (Table 3). The increased isotope effects for the steady-state reactions and the lack of a burst phase in the transient reaction indicate that hydride transfer is significantly rate-limiting for the oxidation of benzyl alcohol by the V292S enzyme. For reduction of benzaldehyde, the isotope effects on V_2/K_p were 2-fold larger for the V292S ADH than for wild-type ADH (Table 3), whereas the isotope effects on V_2 are comparable. The small isotope effect on V_2 and the similar rate constants for turnover (Table 1) and NAD^+ dissociation (Table 3)

Table 2: Product and Dead-End Inhibition Studies for V292S Liver Alcohol Dehydrogenase[a]

inhibitor	substrate: varied	substrate: fixed	pattern	K_{is} (μM)[b]	K_{ii} (μM)[b]
NADH (0−100)	NAD^+ (178−1250)	CH_3CH_2OH (250000)	comp	30	
NAD^+ (0−1000)	NADH (28.5−200)	C_6H_5CHO (970)	comp	1640	
AMP (0−190)	NAD^+ (90−600)	$C_6H_5CH_2OH$ (300)	comp	86	
$C_6F_5CH_2OH$ (0−100)	NAD^+ (71−500)	$C_6H_5CH_2OH$ (1000)	uncomp		1.8
$C_6F_5CH_2OH$ (0−5)	$C_6H_5CH_2OH$ (129−900)	NAD^+ (4000)	comp	2.0	
N-cyclohexylformamide (0−100)	NADH (25−180)	C_6H_5CHO (500)	uncomp		13
N-cyclohexylformamide (0−40)	C_6H_5CHO (240−1800)	NADH (200)	comp	11	

[a] Initial velocities were measured at 25 °C in 33 mM sodium phosphate buffer, pH 8.0, and 0.25 mM EDTA. Concentrations (in μM) are listed in parentheses for each compound. Data were fitted to the equations for competitive (comp) and uncompetitive (uncomp) inhibition, where K_{is} is the slope inhibition constant and K_{ii} is the intercept inhibition constant. [b] K_i values were corrected for the concentration of fixed substrate, yielding the dissociation constants for binding of the inhibitors to the enzyme−coenzyme complexes.

Table 3: Rate Constants and Kinetic Isotope Effects for Native and V292S Enzymes[a]

kinetic parameter	wild-type ADH	V292S ADH
k_{on,NAD^+} ($M^{-1}\,s^{-1}$)	1.2×10^6 [b]	1.1×10^5
k_{off,NAD^+} (s^{-1})	57[b]	220[c]
$k_{on,NADH}$ ($M^{-1}\,s^{-1}$)	1.1×10^7 [b]	7.3×10^6
$k_{off,NADH}$ (s^{-1})	5.5[b]	180[c]
$k_{max,oxidation}$ (s^{-1})[d]	24[b]	6.3
$^Dk_{max,oxidation}$[e]	3.6[b]	4.3
$^DV_1$[e]	1.4 ± 0.1[f]	4.3 ± 0.7
$^DV_2$[e]	1.1 ± 0.1[f]	1.3 ± 0.1
$^DV_1/K_b$[e]	1.6 ± 0.5[f]	3.4 ± 1.2
$^DV_2/K_p$[e]	1.6 ± 0.5[f]	3.1 ± 0.2

[a] Experiments were performed at 25 °C in 33 mM sodium phosphate and 0.25 mM EDTA buffer, pH 8. The errors of the determined values are <25%, unless otherwise indicated. [b] From ref *33*. The k_{on} for NAD^+ binding to wild-type enzyme was calculated using the equation: $k_{on} = k_1k_2/(k_2 + k_{-1})$, using the mechanism in Scheme 1 and the published rate constants (*33*). [c] Calculated from $k_{off} = k_{on}(K_{ia})$ or $k_{on}(K_{iq})$ (Table 1). [d] Maximum rate constant for the transient oxidation of benzyl alcohol (0.16−5 mM) at a fixed concentration of 5 mM NAD^+. [e] The superscript D represents the ratio of kinetic constants with protio and deuterio substrates. [f] From ref *34*.

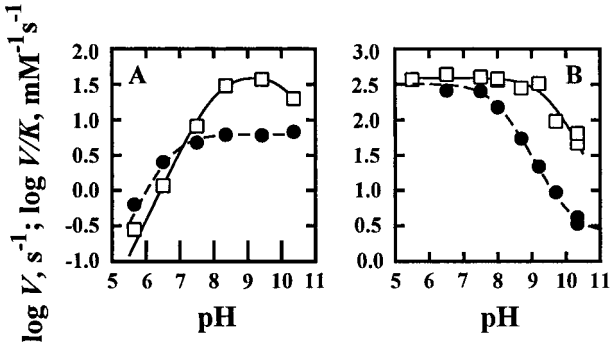

FIGURE 1: pH dependence of benzyl alcohol oxidation and benzaldehyde reduction catalyzed by V292S ADH. (A) Initial velocities for the steady-state oxidation of benzyl alcohol were studied at 25 °C with 4 mM NAD^+ and varied concentrations of alcohol. The V_1 (●) parameter was fit to the equation: $Y_{obs} = Y/(1 + [H^+]/K_1)$, which describes a mechanism in which only unprotonated enzyme reacts with the substrate. The V_1/K_b (□) parameter was fit to the equation: $Y_{obs} = Y/\{1 + ([H^+]/K_1) + (K_2/[H^+])\}$, which describes the mechanism where only singly protonated enzyme reacts with the substrate. The fitted parameters for V_1 gave a pK_1 value of 6.7 ± 0.2 and a limiting value at high pH of 6.2 ± 0.4 s^{-1}. V_1/K_b has two pK_a values, 8.1 ± 0.2 and 10.3 ± 0.1, and a limiting rate at optimal pH of 45 (± 4) $mM^{-1}\,s^{-1}$. (B) The initial velocities of steady-state reduction of benzaldehyde were studied at 25 °C using varied concentrations of benzaldehyde and NADH. V_2 (●) was fitted to the equation: $Y_{obs} = \{Y_1 + (Y_2K_1/[H^+])\}/(1 + K_1/[H^+])$, which describes a mechanism with one K_1 and limiting rates at low pH (Y_2) and high pH (Y_1). V_2/K_p (□) was fitted to the equation: $Y_{obs} = Y/(1 + K_1/[H^+])$, which describes a mechanism in which only the protonated form of the enzyme reacts with the substrate. V_2 has a pK_1 of 8.0 ± 0.2 and a limiting rate at low pH of 320 ± 30 s^{-1} and a limiting rate at high pH of 2.5 ± 20 s^{-1}. V_2/K_p has a pK_1 of 9.5 ± 0.2 and a limiting rate at low pH of 390 ± 30 $mM^{-1}\,s^{-1}$.

suggest that NAD^+ release is the rate-limiting step for the steady-state reduction of benzaldehyde. Fast rates of benzaldehyde reduction by the V292S enzyme precluded a study of the transient reaction.

pH Dependencies. The pH dependencies for the steady-state reactions of the V292S enzyme differ from those for the wild-type enzyme (Figure 1). However, the pK_a for the dependence of V_1 on pH with the V292S enzyme is 6.7, which is similar to the pK_a of 6.4 for the dependence observed for the transient oxidation of benzyl alcohol by the wild-type enzyme (*36*). With the wild-type enzyme, the transient oxidation of benzyl alcohol is controlled by the rate constant for hydride transfer, and the KIE is 3.6 (*33*). The pK_a value for the pH dependence of V_1/K_b is 8.1 for the V292S enzyme. This is lower by about half of a pH unit than the value for the pH dependence of the wild-type enzyme (*34*). The KIEs for benzyl alcohol oxidation (V_1, V_1/K_b) by the V292S enzyme are essentially independent of pH over the pH range of 6.5−10.5. The large isotope effects suggest that the commitments to catalysis are small, and thus the measured pK values approximate the true values for the V292S enzyme complexed with NAD^+ (V_1/K_b) or NAD^+ and benzyl alcohol (V_1) (*37*). The pK_a for the pH dependence of V_2/K_p for the V292S enzyme is lower by 1 pH unit than that of the wild-type enzyme (*34*). The pH dependence of the KIE for V_2/K_p of benzaldehyde reduction by V292S enzyme (data not shown) decreases from a value of 3.1 at pH 7 to a value of 2.6 at pH 9.2. The pK_a of 8.0 for the dependence of V_2 on pH (Figure 1) is the same as that for the wild-type enzyme (*34*). The substitution of an uncharged amino acid residue for another might not be expected to change the pH dependencies for catalysis. However, the differences of 0.5−1 in pK_a values are significant and probably result from changes in rate constants that are affecting macroscopic pK_a values (*37*).

The temperature dependencies of the pH dependencies for V_1 and V_2/K_p were also examined, so that changes in rates due to the temperature dependence of pK_a values could be accounted for. The pK_a for V_1 with the V292S enzyme was found to be temperature-dependent, changing about 0.7 pH unit over a 50 °C temperature range. A van't Hoff plot of the pH dependence for V_1 data at a T_R of 25 °C gave $\Delta H = 9.4 \pm 1.5$ kcal/mol, $\Delta S = -0.03 \pm 4.90$ cal/(mol·K), $\Delta C_p = -0.85 \pm 0.35$ kcal/(mol·K). The ΔH of ionization is similar to that for a histidine [$\Delta H = 6.3$ kcal/mol, $\Delta S = -5.5$ cal/(mol·K); ref *38*] or a water coordinated to zinc ($\Delta H = 11-13$ kcal/mol; ref *37*). The pK_a for the dependence of V_2/K_p on pH did not vary noticeably with temperature.

Temperature Dependencies. The V292S substitution alters coenzyme binding and exposes the hydrogen transfer steps for study by steady-state kinetics. The temperature dependencies for catalysis and the isotope effects were studied in order to evaluate the contribution of protein dynamics and tunneling in the oxidation and reduction reactions catalyzed by V292S ADH. The pH-independent rate constant calculated from the pK_a for V_1 at each temperature was used for the analysis of the temperature dependence of V_1. The data were analyzed in different ways to enable comparisons with the literature. The Eyring plots for V_1 (Figure 2A) show nearly parallel slopes for the protio and deuterio benzyl alcohols with significant values of $\Delta H^‡$, 12.8 kcal/mol, for the protio substrate and a $\Delta H^‡$ of 13.6 kcal/mol for the deuterio substrate (Table 4). The difference in the enthalpy of activations $\Delta\Delta H^‡$ ($\Delta\Delta H^‡ = \Delta H^‡_H - \Delta H^‡_D$) for the substrates is not significant, 0.8 ± 1.0 kcal/mol. The ratio of the Arrhenius preexponential factors (A) for the protio and deuterio substrates is close to unity (1.05 ± 0.46, Table 4). The kinetic isotope effect of 4.1 on V_1 is essentially temperature-independent within the experimental variation of the data (Figure 2B).

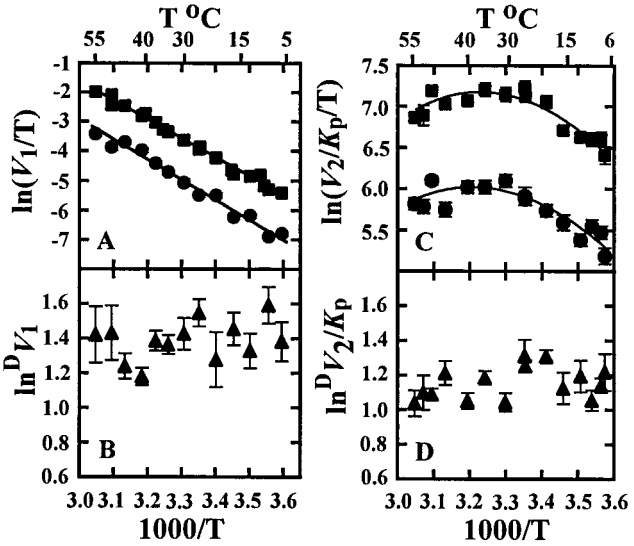

FIGURE 2: Eyring plots for the temperature dependence of V_1 and V_2/K_p for V292S ADH and deuterium isotope effects. The buffers were sodium phosphate, pH 9.2 for V_1 and pH 7.0 for V_2/K_p. (A) Oxidation of benzyl alcohol. V_1 for oxidation of benzyl alcohol (■); V_1 for oxidation of benzyl alcohol-α,α-d_2 (●). (B) Kinetic isotope effect on V_1 for oxidation of benzyl alcohol (▲). (C) Reduction of benzaldehyde. V_2/K_p for reduction of benzaldehyde with NADH (■); V_2/K_p for reduction of benzaldehyde with NADD (●). (D) Kinetic isotope effect on V_2/K_p for reduction of benzaldehyde (▲).

Table 4: Thermodynamic Values from the Temperature Dependence of Reactions Catalyzed by V292S Alcohol Dehydrogenase

Eyring[a]	$\Delta H^{\ddagger}$ (kcal/mol)	$\Delta S^{\ddagger}$ [cal/(mol·K)]	$\Delta G^{\ddagger}$ (kcal/mol), 25 °C
V_1 (H)	12.8 ± 0.5	−12.2 ± 1.8	16.39 ± 0.02
V_1 (D)	13.6 ± 0.9	−12.2 ± 3.0	17.23 ± 0.04

Arrhenius[b]	E_a (kcal/mol)	A (s^{-1})	A_H/A_D
V_1 (H)	13.4 ± 0.2	3.8 (±1.0) × 10^{10}	1.05 ± 0.46
V_1 (D)	14.2 ± 0.9	3.6 (±1.2) × 10^{10}	

van't Hoff[c]	$\Delta H^{\ddagger}$ (kcal/mol)	$\Delta S^{\ddagger}$ [cal/(mol·K)]	$\Delta G^{\ddagger}$ (kcal/mol), 25 °C	$\Delta C_p^{\ddagger}$ [cal/(mol·K)]
V_2/K_p (H)	3.2 ± 0.8	−22.5 ± 2.7	9.89 ± 0.03	−273 ± 89
V_2/K_p (D)	3.2 ± 0.9	−24.6 ± 3.1	10.58 ± 0.04	−236 ± 94

[a] Fitted to the equation: $\ln (k/T) = \ln (k_B/h) + \Delta S^{\ddagger}/R - \Delta H^{\ddagger}/RT$. [b] Fitted to the equation: $\ln k = \ln A - E_a/RT$. [c] Fitted to the equation: $\ln (k/T) = \ln (k_B/h) - (\Delta H^{\ddagger}/RT) + (\Delta S^{\ddagger}/R) + \Delta C_p[-(1/R) + (T_R/RT) + (1/R) \ln (T/T_R)]$, where T_R is the reference temperature, 25 °C.

The Eyring plots for V_2/K_p (Figure 2C) are convex, with an apparent break in the data at about 25 °C. V_2/K_p is temperature-dependent for both protio and deuterio substrates in the range between 5 and 25 °C and temperature-independent from 25 to 50 °C. The data in the two regions can be fitted separately to the Eyring or Arrhenius equations, but the choice of the temperature ranges is somewhat arbitrary, and the errors of the fitted parameters are large (>20%). Thus, we think that the van't Hoff equation is a better way to fit the data, as it describes how V_2/K_p changes over the entire temperature range. The parameters from the fits for the van't Hoff plots for the protio and deuterio substrates are similar (Table 4). The kinetic isotope effect of 3.2 for V_2/K_p is essentially constant over the entire temperature range (Figure 2D). As compared to the KIE of 1.8 determined for the transient reduction of benzaldehyde catalyzed by wild-type enzyme (*33*), the large value of the V_2/K_p kinetic isotope effect for the V292S enzyme suggests that V_2/K_p is controlled by the hydrogen transfer step. Although the kinetic parameters V_1 and V_2/K_p contain different combinations of rate constants, the significant isotope effects indicate that each is controlled by the hydride transfer step. Therefore, the temperature dependencies provide information about the chemistry of the forward and reverse reactions.

Table 5: X-ray Data and Refinement Statistics for V292S Horse Liver Alcohol Dehydrogenase

space group	$P2_1$
cell dimensions, Å	46.3, 180.4, 46.2, $\beta = 107°$
resolution range, Å	20.0−2.0
number of reflections: unique, total	41073, 82843
completeness, % (outer shell)	90.8 (84.9)
R_{sym}, % (outer shell)[a]	3.7 (6.5)
mean $\langle I\rangle/\sigma\langle I\rangle$ (outer shell)	11.4 (8.9)
R_{value}, R_{free}, test %[b]	0.197, 0.231, 1.5
rsmd for bond distances[c]	0.012
rmsd for bond angles	1.53
no. of water molecules per dimer	164

[a] $R_{sym} = (\Sigma|I - \langle I\rangle|)/\Sigma\langle I\rangle$, where I is the integrated intensity of a given reflection. [b] $R_{value} = (\Sigma||F_o| - k|F_c||/\Sigma|F_o|$, where k is a scale factor. The R_{free} (*39*) values were calculated with the indicated percentage of reflections not used in the refinement. [c] Root-mean-square deviations (rmsd) from the ideal geometry of the final model.

X-ray Crystallography. The structure of the V292S enzyme was determined in order to evaluate the basis for the large changes in kinetic constants. The X-ray data collection and refinement statistics are summarized in Table 5. The V292S enzyme has the entire dimeric molecule in the asymmetric unit, but the three-dimensional structure of each subunit is very similar to that of the native apo-enzyme crystallized in the absence of ligands (*40*). The V292S enzyme structure is closely superimposable on the native apo-enzyme (rmsd = 0.37 Å) and the G293A/P295T enzyme (rmsd = 0.23 Å) (*41*), which are both found to be in the "open" form. The electron density map around the V292S substitution confirms the mutation and shows the quality of the final refined electron density map (Figure 3). The hydroxyl of Ser-292 is hydrogen-bonded to a water molecule (Wat 1) that makes contacts with the carbonyl oxygen of Val-290 (Figure 3); this water molecule fills space that is created by the V292S substitution.

The V292S enzyme was crystallized in the presence of NAD^+ and 2,3,4,5,6-pentafluorobenzyl alcohol, but electron density was observed only for the ADP portion of the coenzyme. No electron density is observed for the nicotinamide riboside of NAD^+ or the 2,3,4,5,6-pentafluorobenzyl alcohol. The active site zinc has a water molecule as its fourth ligand.

When wild-type enzyme is crystallized in the presence of NAD^+ and 2,3,4,5,6-pentafluorobenzyl alcohol, the enzyme is in a "closed" form, which results from a rotation of about 10° of the catalytic domain toward the coenzyme binding domain (*1*). Although the V292S enzyme was crystallized in the presence of NAD^+ and 2,3,4,5,6-pentafluorobenzyl alcohol at concentrations high enough to saturate the active

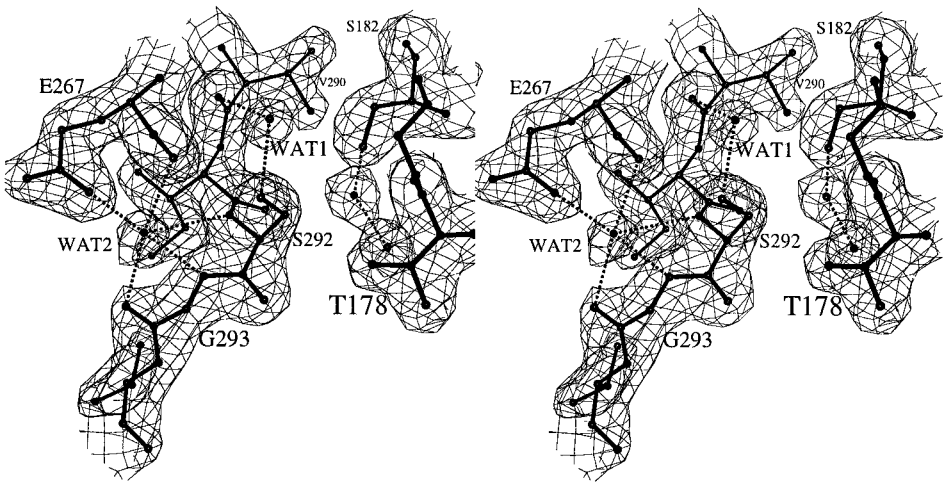

FIGURE 3: Structure of the region with the V292S substitution. The final $2|F_o - F_c|$ electron density map covering residues 290−294 and 267 and bound waters is shown (contoured at 1σ).

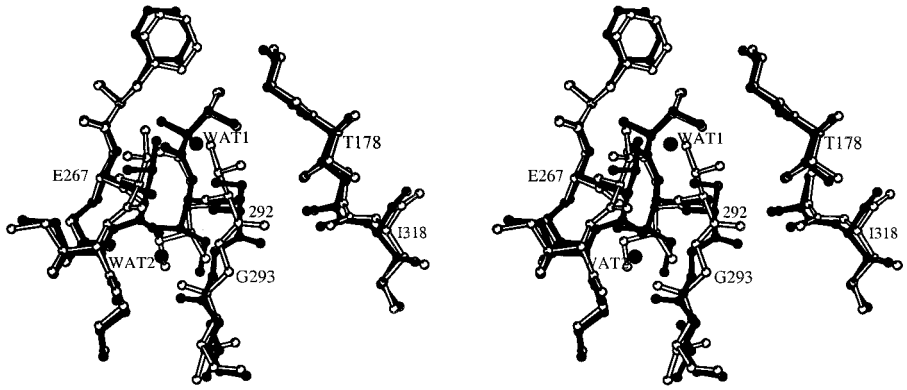

FIGURE 4: Comparison of the V292S and apo-enzyme structures. The coenzyme binding domains of the V292S enzyme (in black, PDB entry 1JU9) and apo-enzyme (unfilled, PDB entry 8adh) were superimposed using program *O*. The changes in conformation of residues 290−294, 263−268, 178, and 317−318 are shown.

sites, the V292S enzyme is in the open conformation of the apo and G293A/P295T enzymes. The structural basis for the effect of the mutation on the conformational change is not obvious from a comparison of the structures.

The main differences between the V292S and the apo-enzyme structures are local effects due to the mutation (Figure 4). The side chain of Ser-292 does not overlap the atoms of Val-292 in the wild-type enzyme, and the side chain of Ile-291 has different rotamer conformations in the two enzymes. In the V292S structure, the residues of the catalytic domain are shifted slightly (about 0.25 Å) more toward the coenzyme binding domain, as compared to the structure of the native apo-enzyme, resulting in a more closed conformation (Figure 4). The difference may result from the V292S substitution or from crystallization under different conditions. The V292S enzyme was crystallized at pH 7 in the presence of NAD^+, whereas the apo-enzyme was crystallized at pH 8.4 without nucleotide. The apo and V292S enzymes crystallize in different space groups.

DISCUSSION

Effects of the V292S Substitution on Structure and Mechanism. Modeling the V292S substitution in the structure of a ternary complex of native ADH (*1*) suggested that removal of a methyl group would create more space behind the nicotinamide ring of bound NAD^+ and might decrease the rate of hydride transfer due to perturbed interactions with the nicotinamide ring. Indeed, the rate constant for alcohol oxidation decreases somewhat with the V292S enzyme (Table 3), but the large effect of the substitution on coenzyme binding and the perturbation of the enzyme conformational change were unexpected.

The V292S substitution does not affect the binding of AMP, but decreases the affinity for NAD^+ and NADH by at least 50-fold. This suggests the V292S enzyme forms the initial complex with coenzyme, but does not readily undergo the conformational change. In wild-type ADH, residue 292 is located at the beginning of a loop of the coenzyme binding domain that moves upon the binding of coenzyme and allows the catalytic and coenzyme binding domains to come closer together. The Val to Ser substitution may reduce the hydrophobic interactions with the nicotinamide ring so that the ring is less tightly bound and can only stabilize the closed conformation to a limited extent. Interactions with the nicotinamide ring are critical for the conformational change, since the enzyme crystallized with ADP-ribose is in the open conformation (*42*).

As illustrated in Scheme 1, the binding of NAD^+ is a two-step process, with an isomerization that apparently corresponds to the conformational change observed by X-ray crystallography. For wild-type enzyme, rate constants have been calculated from analysis of transient data for the binding

Scheme 1

$$E + A \underset{k_{-1}}{\overset{k_1}{\rightleftharpoons}} EA \underset{k_{-2}}{\overset{k_2}{\rightleftharpoons}} FA$$

of NAD^+ with values of 620 s^{-1} for k_2 and 65 s^{-1} for k_{-2} (*33*). For the V292S enzyme, a similar analysis was not possible because a limiting rate for complex formation was not observed (up to 200 s^{-1}). Nevertheless, the alterations in the dissociation constant for NAD^+ (K_{ia}, Table 1), the turnover number (V_2, Table 1), and the overall rate constant for binding of NAD^+ (k_{on}, Table 3) indicate the rate constants in Scheme 1 are affected by the V292S substitution. Values that are reasonable and consistent with the observed kinetic parameters are $k_1 = 4.7 \times 10^7$ M^{-1} s^{-1}, $k_{-1} = 2.8 \times 10^5$ s^{-1}, $k_2 = 690$ s^{-1}, and $k_{-2} = 240$ s^{-1}. The rate constants indicate that the V292S substitution has decreased the equilibrium constant for step 2 by about 3-fold and increased the rate constants for dissociation, k_{-1} and k_{-2}, 12-fold and 3.7-fold, respectively. Although the equilibrium position for step 2 should favor the isomerized complex (FA), and binding of a substrate or inhibitor to the enzyme−NAD^+ complex could also affect the conformation, the three-dimensional structure is open in the crystals. Crystal lattice contacts seem to be sufficient to perturb the delicate equilibrium.

The propensity of the V292S enzyme to be in the open conformation explains the low affinity for coenzyme, but raises the question of whether the enzyme assumes a closed conformation when the ternary Michaelis complex forms. The inhibition constants for the dead-end inhibitors *N*-cyclohexylformamide and 2,3,4,5,6-pentafluorobenzyl alcohol and the catalytic efficiencies with benzyl alcohol and benzaldehyde (V_1/K_b, V_2/K_p) are very similar to those for the wild-type enzyme. This suggests that the substrate binding sites for the V292S and wild-type enzymes are very similar and that the V292S enzyme can adopt a closed conformation in the enzyme−coenzyme complex. Since the conformational change with wild-type enzyme affects the substrate binding pocket, we expect that the inhibition constants should be different if the V292S enzyme remains in the open conformation during catalysis. The ADH enzymes that have the G293A/P295T substitutions (*41*) or isonicotinimidylated lysines (*43*) also crystallize in the open form with coenzyme bound. The catalytic efficiencies of these two enzymes are very different from those of the wild-type enzyme and are thought to stay in the open conformation during catalysis. The G293A/P295T enzyme has a K_i for 2,3,4,5,6-pentafluorobenzyl alcohol of 3 mM, 10^3-fold higher than the K_i with the V292S enzyme. Thus, we suggest that the V292S enzyme has a closed conformation during hydride transfer.

Substitution of Val-203, which is adjacent to Val-292 and also near the nicotinamide ring, with Ala creates more space behind the nicotinamide ring. However, the structure of the V203A−NAD^+−2,2,2-trifluoroethanol complex is in the closed form, with catalytic and coenzyme domains 0.5 Å closer than they are in the wild-type structure (*14*). The V203A and wild-type enzymes bind coenzyme with similar affinities. The V203A mutation reduces the hydrophobic interactions with the nicotinamide ring, but Val-203 may not be in a position to affect the conformation of the enzyme, unlike Val-292 which is adjacent to the flexible loop with residues 293−298 that need to rearrange during the conformational change.

Catalytic Dynamics. TheV292S substitution increases the rates of dissociation of coenzyme and unmasks the hydride transfer step while the catalytic efficiencies (*V/K*) remain similar to those of the wild-type enzyme. Previously, substitutions in the substrate binding site were found to unmask hydride transfer and hydrogen tunneling (*13*). The substitutions change rate-limiting steps so that significant isotope effects become apparent and the mechanisms of catalysis can be probed more readily than with the wild-type enzyme.

The temperature dependence of benzyl alcohol oxidation (V_1) by V292S ADH shows parallel dependencies for the protio and deuterio substrates with significant $\Delta H^{\ddagger}$ values of about 13 kcal/mol (Table 4) and no experimentally significant temperature dependence of the kinetic isotope effect (Figure 2B). Temperature-independent isotope effects are seen with reactions that occur through ground-state hydrogen tunneling, but these reactions usually have very small $\Delta H^{\ddagger}$ values (*44*). Temperature-independent isotope effects and significant $\Delta H^{\ddagger}$ values have been observed with *Bacillus stearothermophilus* alcohol dehydrogenase (*12*), sarcosine oxidase (*45*), Δ^9-desaturase (*46*), methylamine dehydrogenase (*47*), aromatic amine dehydrogenase (*48*), and trimethylamine dehydrogenase (*49*). The temperature dependence data for the reductive half-reaction of ethanolamine by methylamine dehydrogenase closely resemble the V_1 data for the V292S enzyme (significant $\Delta H^{\ddagger}$ values and essentially temperature-independent isotope effects). The kinetics of these enzymes have been explained with vibrationally assisted tunneling models, which use a fluctuating potential energy barrier (*3*−*8*, *50*).

In these models, thermal fluctuations alter the symmetry and the distance between the product and reactant wells (*3*−*5*). These thermal fluctuations come from the natural motions of the substrates and protein and affect catalysis either by changing the distance between the reactants or by exciting productive vibrations. Because the fluctuations decrease the width of the energy barrier, the hydrogen atom can tunnel. With vibrationally assisted tunneling, the $\Delta H^{\ddagger}$ represents the enthalpy of an energy barrier that must be overcome in order to preorganize the substrates and active site so that hydrogen transfer can occur. This preorganization energy is temperature-dependent and isotope-independent (*3*, *4*). We think that the vibrationally assisted tunneling model best describes the data for the temperature dependence for the oxidation of benzyl alcohol by V292S ADH. A corner-cutting model is not consistent with the significant magnitude for $\Delta H^{\ddagger}$ and the temperature-independent isotope effect (*3*, *10*, *50*).

The temperature dependence of benzaldehyde reduction (V_2/K_p) was analyzed by fitting all of the data to the van't Hoff equation, which rigorously takes into account the temperature dependence of $\Delta H^{\ddagger}$, or heat capacity (ΔC_p). The temperature-independent KIE (Figure 2D) is consistent with the ground-state and vibrationally assisted tunneling models, but not with the semiclassical or the rigid-barrier tunneling models of hydride transfer. The nonlinear temperature dependence is also consistent with the vibrationally assisted tunneling model (*50*). The significant $\Delta C_p^{\ddagger}$ value for the benzaldehyde reduction by V292S ADH (Table 4) suggests that protein fluctuations or conformational changes affect the

organization of the reactants (*51*). The similar, small enthalpic contributions for protio and deuterio substrates obtained from the van't Hoff fits indicate that thermal activation is a modest contributor to the reaction. As the temperature of the reaction increases, the enzyme may favor a state that is functionally preorganized for tunneling over a state that has a higher enthalpy for preorganization, resulting in a nonlinear temperature dependence.

Some other enzymes have nonlinear temperature dependencies, which can be explained by various mechanisms (*12*, *51*−*53*). Convex temperature dependencies for both V_1 and V_1/K_b have also been observed for the oxidation of benzyl alcohol by *Bacillus stearothermophilus* alcohol dehydrogenase (*12*). With the *Bacillus* ADH, the extent of tunneling increases with temperature up to a transition at about 30 °C, and above that temperature the data are consistent with a vibrationally assisted tunneling model. The nonlinear behavior for benzaldehyde reduction by V292S ADH is conceivably due to relative changes in the rate constants that comprise V_2/K_p. However, the isotope effect is temperature-independent, and the rate constants would have to change fortuitously so that the commitments to catalysis did not change. With the V292S enzyme, the temperature-independent KIE for V_2/K_p, the large $\Delta C_p^{\ddagger}$, and the similar $\Delta H^{\ddagger}$ values for the protio and deuterio substrates are consistent with the vibrationally assisted tunneling model.

The temperature dependencies for the forward and reverse reactions do not resemble each other, which may be expected for reactions that have different substrates and rate constants. The oxidation and reduction reactions could involve different substates of the enzyme. Different energetics are observed for the turnover of different substrates by aromatic amine dehydrogenase (*48*). Changes in protein dynamics with different substrate complexes have been observed with molecular dynamics studies. Simulations with ternary complexes of dihydrofolate reductase showed the protein motions of the dihydrofolate reductase−dihydrofolate−NADPH complex differed significantly from the motions of the dihydrofolate reductase−tetrahydrofolate−$NADP^+$ complex (*54*). Distortion of the oxidized and reduced nicotinamide ring has been implicated in the reactions catalyzed by ADH (*55*, *56*). Such distortion can decrease the distance between the reactants, which facilitates tunneling, and could better align the molecular orbitals of the atoms involved in the transfer. The difference in preorganization enthalpies between the oxidation and reduction reactions of the V292S enzyme could be due to the puckering of the nicotinamide ring that occurs in the formation of the transition state or preorganized ground state. The oxidized nicotinamide ring of NAD^+ is aromatic and may require more energy to cause a puckering in the ring as compared to the dihydronicotinamide ring of NADH; a larger preorganization energy may reflect this energetic difference.

The present studies provide evidence for a role of protein dynamics in both the oxidation of alcohols and the reduction of aldehydes. Although the V292S ADH has altered coenzyme binding, the rates of hydride transfer and catalytic efficiencies are not greatly affected, indicating that Val-292 is not the only residue that contributes to catalysis. Future studies are required to develop theoretical models that quantitatively explain the data.

ACKNOWLEDGMENT

We thank Professor Amnon Kohen for valuable discussions and The University of Iowa Macromolecular Crystallography Facility for instrumentation.

REFERENCES

1. Ramaswamy, S., Eklund, H., and Plapp, B. V. (1994) *Biochemistry 33*, 5230−5237.
2. Ramaswamy, S., Scholze, M., and Plapp, B. V. (1997) *Biochemistry 36*, 3522−3527.
3. Kohen, A., and Klinman, J. P. (1999) *Chem. Biol. 6*, R191−R198.
4. Sutcliffe, M. J., and Scrutton, N. S. (2000) *Trends. Biochem. Sci. 25*, 405−408.
5. Antoniou, D., and Schwartz, S. D. (1997) *Proc. Natl. Acad. Sci. U.S.A. 94*, 12360−12365.
6. Antoniou, D., and Schwartz, S. D. (1998) *J. Chem. Phys. 108*, 3260−3265.
7. Borgis, D., and Hynes, J. T. (1991) *J. Chem. Phys. 94*, 3619−3628.
8. Bruno, W. J., and Bialek, W. (1992) *Biophys. J. 63*, 689−699.
9. Kuznetsov, A. M., and Ulstrup, J. (1999) *Can. J. Chem. 77*, 1085−1096.
10. Melander, L., and Saunders, W. H. (1987) in *Reaction Rates of Isotopic Molecules*, pp 140−169, R. E. Krieger Publishing Co., Malabar, FL.
11. Cha, Y., Murray, C. J., and Klinman, J. P. (1989) *Science 243*, 1325−1330.
12. Kohen, A., Cannio, R., Bartolucci, S., and Klinman, J. P. (1999) *Nature 399*, 496−499.
13. Bahnson, B. J., Park, D.-H., Kim, K., Plapp, B. V., and Klinman, J. P. (1993) *Biochemistry 32*, 5503−5507.
14. Bahnson, B. J., Colby, T. D., Chin, J. K., Goldstein, B. M., and Klinman, J. P. (1997) *Proc. Natl. Acad. Sci. U.S.A. 94*, 12797−12802.
15. Ganzhorn A. J., and Plapp, B. V. (1988) *J. Biol. Chem. 242*, 4275−4278.
16. Park, D.-H., and Plapp, B. V. (1991) *J. Biol. Chem. 266*, 13296−13320.
17. Theorell, H., and Yonetani, T. (1964) *Biochem. Z. 338*, 537−553.
18. Plapp, B. V. (1970) *J. Biol. Chem. 245*, 1727−1735.
19. Cleland, W. W. (1979) *Methods Enzymol. 63*, 103−138.
20. Johnson, M. L., and Frasier, S. G. (1985) *Methods Enzymol. 117*, 301−342.
21. Leslie, A. G. W. (1992) in *Joint CCP4 and ESF-EACMB Newsletters on Protein Crystallography No. 26*, Daresbury Laboratory, Warrington, U.K.
22. CCP4 Suite (1994) *Acta Crystallogr., Sect. D D50*, 760−763.
23. Navaza, J. (1994) *Acta Crystallogr. 50*, 157−163.
24. Brunger, A. T., Adams, P. D., Clore, G. M., DeLano, W. L., Gros, P., Grosse-Kunstlev, R. W., Jaing, J. S., Kusezewski, J. T., Nilges, M., Pannu, N. S., Read, R. J., Rice, L. M., Simonson, T., and Warren, G. L. (1998) *Acta Crystallogr., Sect. D D54*, 905−921.
25. Jones, T. A., Zou, J. Y., Cowan, S. W., and Kjeldgaard, M. (1991) *Acta Crystallogr., Sect. A A47*, 110−119.
26. Vriend, G. (1990) *J. Mol. Graphics 8*, 52−56.
27. Laskowski, R. A., MacArthur, M. W., Moss, D. S., and Thorton, J. M. (1993) *J. Appl. Crystallogr. 26*, 283−290.
28. Klinman, J. P. (1972) *J. Biol. Chem. 247*, 7977−7987.
29. Weidig, C. F., Halvorson, H. R., and Shore, J. D. (1977) *Biochemistry 16*, 2916−2922.
30. Dunn, M. F., Bernhard, S. A., Anderson, D., Copeland, A., Morris, R. G., and Roque, J.-P. (1979) *Biochemistry 18*, 2346−2354.
31. Shearer, G. L., Kim, K., Lee, K. M., Wang, C. K., and Plapp, B. V. (1993) *Biochemistry 32*, 11186−11194.
32. Fan, F., and Plapp, B. V. (1995) *Biochemistry 34*, 4709−4713.

33. Sekhar, V. C., and Plapp, B. V. (1990) *Biochemistry 29*, 4289−4295.
34. Dworschack, R. T., and Plapp, B. V. (1977) *Biochemistry 16*, 2716−2725.
35. Dalziel, K. (1963) *J. Biol. Chem. 238*, 2850−2858.
36. Kvassman, J., and Pettersson, G. (1978) *Eur. J. Biochem. 87*, 417−427.
37. Cleland, W. W. (1977) *Adv. Enzymol. Relat. Areas Mol. Biol. 45*, 273−387.
38. *CRC Handbook of Biochemistry* (1970) 2nd ed., p J-116, The Chemical Rubber Co., Cleveland, OH.
39. Brunger, A. T. (1992) *Nature 335*, 472−474.
40. Eklund, H., Nordström, B., Zeppezauer, E., Söderlund, G., Ohlsson, I., Boiwe, T., Söderberg, B.-O., Tapia, O., Brändén, C.-I., and Åkeson, Å. (1976) *J. Mol. Biol. 102*, 27−59.
41. Ramaswamy, S., Park, D.-H., and Plapp, B. V. (1999) *Biochemistry 38*, 13951−13959.
42. Eklund, H., Samama, J.-P., and Jones, T. A. (1984) *Biochemistry 23*, 5982−5996.
43. Plapp, B. V., Eklund, H., Jones, T. A., and Brändén, C.-I. (1983) *J. Biol. Chem. 258*, 5537−5547.
44. Jonsson, T., Glickman, M. H., Sun, S., and Klinman, J. P. (1996) *J. Am. Chem. Soc. 118*, 10319−10320.
45. Harris, R. J., Meskys, R., Sutcliffe, M. J., and Scrutton, N. S. (2000) *Biochemistry 39*, 1189−1198.
46. Abad, J. L., Camps, F., and Fabriàs, G. (2000) *Angew. Chem., Int. Ed. Engl. 39*, 3279−3281.
47. Basran, J., Sutcliffe, M. J., and Scrutton, N. S. (1999) *Biochemistry 38*, 3218−3222.
48. Basran, J., Patel, S., Sutcliffe, M. J., and Scrutton, N. S. (2001) *J. Biol. Chem. 276*, 6234−6242.
49. Basran, J., Sutcliffe, M. J., and Scrutton, N. S. (2001) *J. Biol. Chem. 276*, 24581−24587.
50. Antoniou, D., and Schwartz, S. D. (2001) *J. Phys. Chem. B 105*, 5553−5558.
51. Eftink, M. R., and Biltonen, R. L. (1983) *Biochemistry 22*, 5140−5150.
52. Borgman, U., Moon, T. W., and Laidler, K. J. (1974) *Biochemistry 13*, 5152−5158.
53. Truhlar, D. G., and Kohen, A. (2001) *Proc. Natl. Acad. Sci. U.S.A. 98*, 848−851.
54. Radkiewicz, J. L., and Brooks, C. L. (2000) *J. Am. Chem. Soc. 122*, 225−231.
55. Luo, J., Kahn, K., and Bruice, T. C. (1999) *Bioorg. Chem. 27*, 289−296.
56. Webb, S. P., Agarwal, P. K., and Hammes-Schiffer, S. (2000) *J. Phys. Chem. B 104*, 8884−8894.

BI011540R